REPORT DOCUMENTATION PAGE

Form Approved
OMB No. 0704-0188

1. REPORT DATE *(DD-MM-YYYY)*	2. REPORT TYPE	3. DATES COVERED *(From - To)*
04 May 2012	Conference Paper and Briefing Slides	

4. TITLE AND SUBTITLE

Detectability of Delaminations in Solid Rocket Motors with Embedded Stress Sensors

5a. CONTRACT NUMBER

5b. GRANT NUMBER

5c. PROGRAM ELEMENT NUMBER

6. AUTHOR(S)
Anhduong Q. Le, L.Z. Sun, and Timothy C. Miller

5d. PROJECT NUMBER

5f. WORK UNIT NUMBER
Q09Y

7. PERFORMING ORGANIZATION NAME(S) AND ADDRESS(ES)

Air Force Research Laboratory (AFMC)
AFRL/RZSM
9 Antares Road
Edwards AFB CA 93524-7401

8. PERFORMING ORGANIZATION REPORT NUMBER

9. SPONSORING / MONITORING AGENCY NAME(S) AND ADDRESS(ES)

Air Force Research Laboratory (AFMC)
AFRL/RZS
5 Pollux Drive
Edwards AFB CA 93524-7048

10. SPONSOR/MONITOR'S ACRONYM(S)

11. SPONSOR/MONITOR'S NUMBER(S)
AFRL-RZ-ED-TP-2012-074

12. DISTRIBUTION / AVAILABILITY STATEMENT

Distribution A: Approved for public release; distribution unlimited.

13. SUPPLEMENTARY NOTES

Presented at the JANNAF Joint Propulsion Meeting in San Antonio, TX, 30 Apr – 4 May 2012.
PA# 12222 (Conference paper) and PA#12225 (Briefing slides).

14. ABSTRACT

A finite-element-based numerical model is employed to investigate the effect of propellant-insulation delaminations on the radial stress distribution at the bondline during the cooling of a solid rocket motor consisting of propellant, insulation, and casing. With the assumption of stress sensors evenly distributed along the propellant-insulation interface, the way that the debond angles, number of sensors, and sensor accuracy are related is established. Two approaches are proposed to evaluate the detectability of debonds based on the sensor readings. Furthermore, a quantitative mapping obtained between the debond angle and the sensor data is used to inversely estimate the delamination damage. It is demonstrated that the proposed methods can be used to detect delaminations in solid rocket motors.

15. SUBJECT TERMS

16. SECURITY CLASSIFICATION OF:			17. LIMITATION OF ABSTRACT	18. NUMBER OF PAGES	19a. NAME OF RESPONSIBLE PERSON
					Dr. Timothy C. Miller
a. REPORT	b. ABSTRACT	c. THIS PAGE			19b. TELEPHONE NUMBER *(include area code)*
Unclassified	**Unclassified**	**Unclassified**	SAR	27	N/A

DETECTABILITY OF DELAMINATIONS IN SOLID ROCKET MOTORS WITH EMBEDDED STRESS SENSORS

Anhduong Q. Le and L. Z. Sun
University of California, Irvine, CA 92697-2175
Timothy C. Miller
Air Force Research Laboratory, Edwards AFB, CA 93524

ABSTRACT

A finite-element-based numerical model is employed to investigate the effect of propellant-insulation delaminations on the radial stress distribution at the bondline during the cooling of a solid rocket motor consisting of propellant, insulation, and casing. With the assumption of stress sensors evenly distributed along the propellant-insulation interface, the way that the debond angles, number of sensors, and sensor accuracy are related is established. Two approaches are proposed to evaluate the detectability of debonds based on the sensor readings. Furthermore, a quantitative mapping obtained between the debond angle and the sensor data is used to inversely estimate the delamination damage. It is demonstrated that the proposed methods can be used to detect delaminations in solid rocket motors.

INTRODUCTION

Structural health monitoring is one strategy for improving the safety and reliability of solid rocket motors (SRMs).[1,2] The ability to detect damage in SRMs will help enable timely, accurate, and reliable assessments of structural integrity, which will yield great cost savings and help prevent catastrophic structural failures.[3] Currently, due to uncertainties associated with service life predictions, many SRMs must be disposed of prematurely. A fundamental understanding of how diurnal or seasonal temperature cycles affect rocket motors and cause related defects is critical for the development of improved service life predictions for rocket motors.

Because SRMs are cooled from the cure temperature to ambient temperatures, radial stresses persist in the grain throughout its life, the continuous stresses can cause critical flaws that result in catastrophic ignition failure. There are three important grain-related failure mechanisms: propellant aging,[4-8] bore cracking,[9-11] and delaminations (debonds) at the interfaces between the propellant, insulation, and case.[12] Little research has focused on using health monitoring to detect this last type of defect, although recently Brouwer et al. illustrated the effect of debonds on radial stress distributions along the bondline between the propellant and the casing.[12] In this paper, we use the finite element method to investigate the effect of delaminations on the radial stress distribution at the bondline during the cooling process of a solid rocket motor consisting of propellant, insulation, and casing. We establish a relationship between the debond angle, the number of sensors, and the required sensor accuracy. Included is a method to estimate the debond size from the sensor data. It is demonstrated that the proposed methodology can successfully detect delaminations in solid rocket motors.

FINITE ELEMENT MODEL DETAILS

The solid rocket motor considered is shown in Figure 1. The inner and outer grain diameters are 203.2 mm and 406.4 mm, respectively. The insulation and case are 2.54 mm and 3.175 mm thick, respectively. The propellant is a typical HTPB/AP composite grain with an EPDM insulation layer. The temperature-dependent elastic mechanical properties of HTPB/AP and EPDM were obtained from in-house testing at AFRL/RZSM (Edwards AFB). The motor case is assumed to be a filament-wound graphite-epoxy motor. A simplified symmetric layup with winding angles of $(0^\circ/90^\circ/\pm45^\circ)_s$ is assumed and modeled with quasi-isotropic properties.[13]

Most SRMs are designed with stress-relieving slots and flaps or boots near the ends of the grain. Therefore, we assumed the typical delamination nucleates at the midplane of the motor, where high stress triaxiality conditions dominate (as the damage progresses, the delamination propagates longitudinally). The corresponding plane-strain problem can be analyzed using finite element analysis to investigate the effect of a debond on the local stress distribution. The analysis is performed using the

commercially available finite element software package Abaqus.[14] Four specific debond cases are considered: the debonds subtend arcs with total angles of 5˚, 10˚, 15˚, and 20˚ (denoted by α in Section A-A of Figure 1). All cases are subjected to slow temperature cooling from the cure temperature down to a specified service temperature. A stress-free cure temperature of 60˚C is assumed with a final service temperature of -40˚C, giving a total temperature drop of 100˚C.

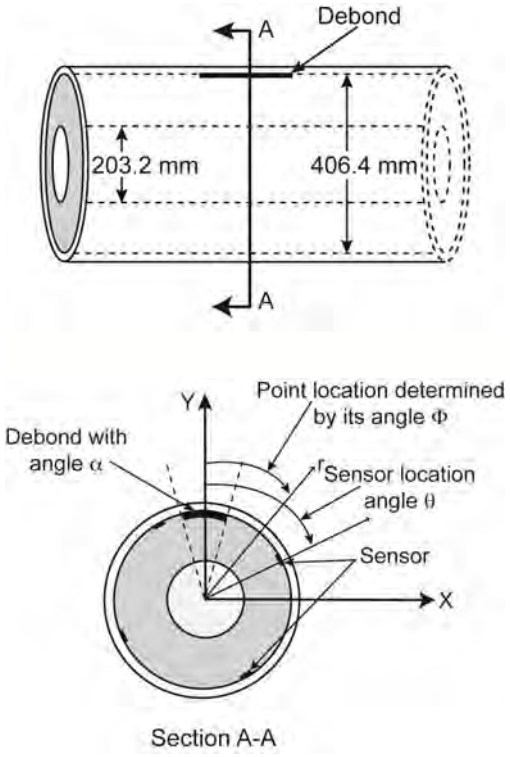

Figure 1: Schematic diagram of a solid rocket motor showing a delamination and an array of four stress and temperature sensors at the motor midplane

Plane-strain finite element models of solid rocket motors with total debond angles of 5˚, 10˚, 15˚, and 20˚ were analyzed – a typical mesh, shown in Figure 2, has a total debond angle of 20˚ (due to symmetry conditions, only half of the cross-section is modeled). The tip of the delamination is modeled as an interfacial crack tip with a heavily refined mesh. The elements were quadratic isoparametric hybrid elements with reduced-order integration.* Displacement boundary conditions prevent horizontal motion along the left edge and prevent vertical motion at a single node, so that rigid body motion is inhibited. The stresses at the propellant/insulation surface are calculated for temperatures from 60 C to -40˚C (cooling takes place in a quasistatic fashion with 10˚C increments). A convergence study confirmed that the level of mesh refinement used in this paper was adequate.

* The finite element software, Abaqus, employs what are referred to in its literature as “hybrid elements.” These elements incorporate pressure as an independent variable, to help prevent convergence problems associated with models that include incompressible or nearly incompressible materials.

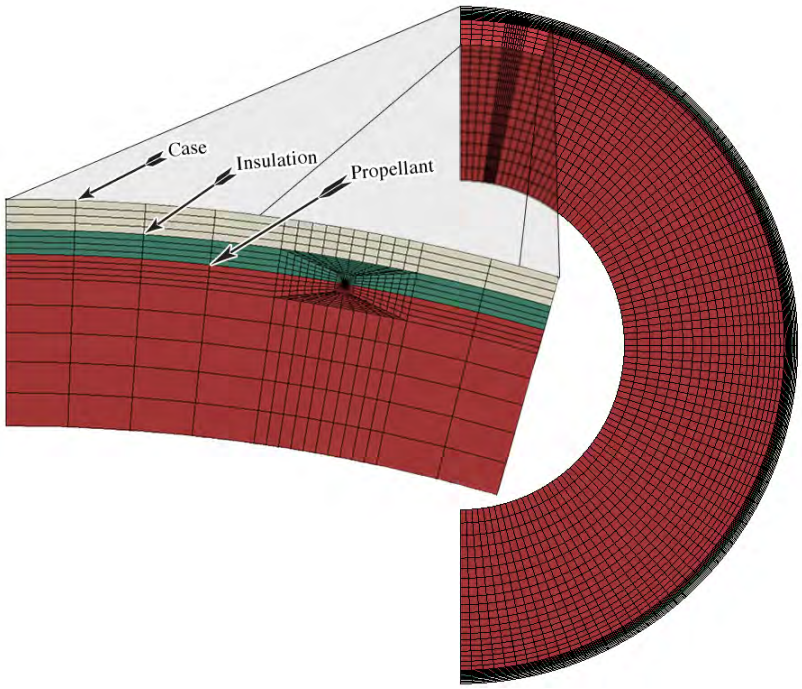

Figure 2: A finite element mesh of the motor midplane. The model shown here has a total debond angle of 10 degrees.

RESULTS AND DISCUSSION

Figure 3 shows the Dual Bond Stress and Temperature (DBST) sensor that is proposed for health monitoring of solid rocket motors.[15,16] These sensors have been designed specifically for this purpose, and measure both radial stress (bond stress) and temperature near the case wall. Both wired and wireless prototypes are being developed. Long-term testing and iterative improvements in the manufacturing process have improved accuracy to at least 10 kPa, but significantly greater accuracy is expected due to advances in design and manufacture. Since the sensors measure radial stresses near the case wall, we focused on analysis of radial stresses. In addition, although the presence of a debond clearly perturbs the stresses through the entire cross-section, this work focuses on radial stresses adjacent to the bondline, since these correlate with sensor measurements. Figure 4 shows a typical finite element model contour plot of radial stress near the tip of a delamination with a total debond angle of 20˚ at a temperature of -40˚C.

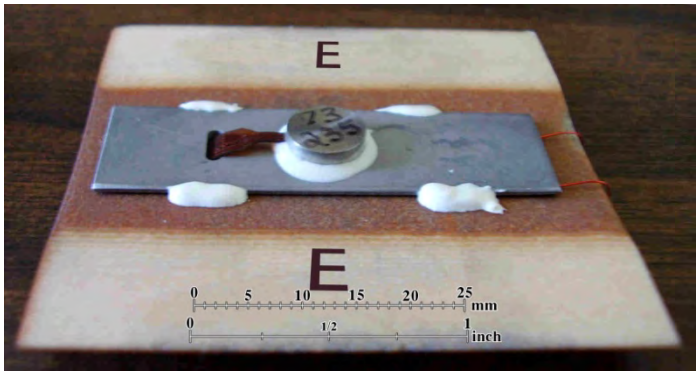

Figure 3: A dual bond-stress and temperature sensor mounted on a phenolic shim

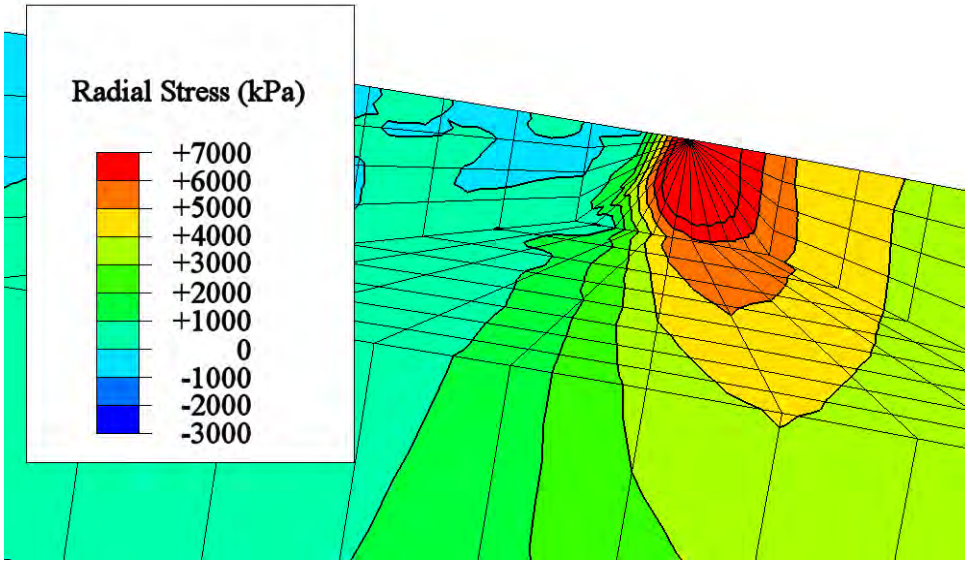

Figure 4: Distribution of radial stress at the tip of a 20˚ total debond at -40˚C

Figure 5 shows the radial stress distribution over the circumference of the grain of the solid rocket motors in four different debond cases with different debond angles (α = 5˚, 10˚, 15˚, and 20˚). The horizontal line at 855 kPa is the baseline radial stress for a defect-free motor. Obviously, at points remote from the defect, the radial stress approaches its baseline value.

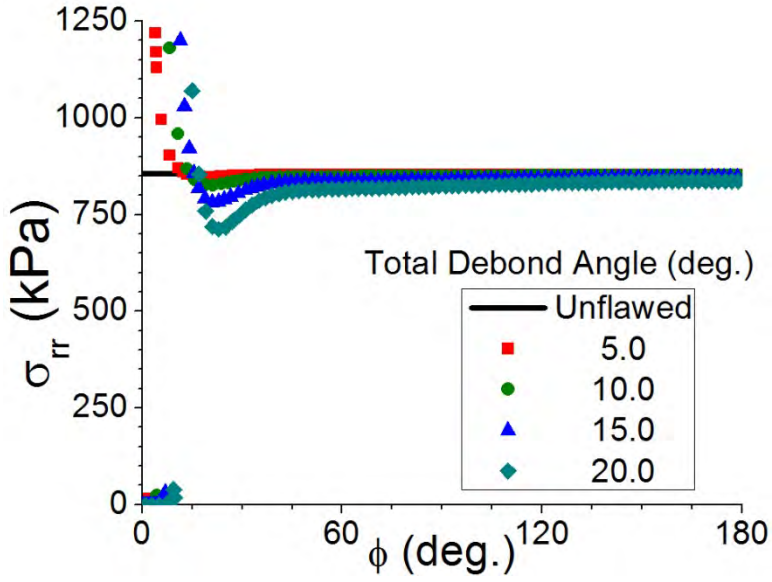

Figure 5: Radial stresses along the edge of the propellant grain for various debond sizes (total debond angles of 5˚, 10˚, 15˚, and 20˚).

Structural health monitoring can play an important role in detecting rocket motor delaminations. Stress sensors can be embedded at the bondline to measure radial stress around the edge of the propellant grain. Four sensors are first assumed to be evenly mounted with a 90˚ circumferential angle between any two neighbors. Their function is to monitor radial stresses, since changes can indicate the presence of a defect. For the detection of debonds, the maximum and minimum values of four sensor readings are compared – the difference between the highest and lowest radial stresses for various positions of the sensor set is determined (i.e., the position of the sensor set is characterized by θ in

Figure 1). The least optimal location (corresponding to the smallest value of these differences) is compared with sensor accuracy for various defect sizes. In Figure 6, for example, analysis for a 20˚ debond angle is shown. The smallest difference between maximum and minimum stress values of the four sensors takes place if θ = 45˚, and this difference is 22.7 kPa. In other words, no matter where the sensors are located, the difference between the maximum and the minimum values of the four sensor readings is always larger than 22.7 kPa. For the sensors currently being considered, the stress values are accurate to ±10 kPa.[15,16] The implication is that defects with 20˚ debond angles in this solid rocket motor could be detected with 100% reliability.

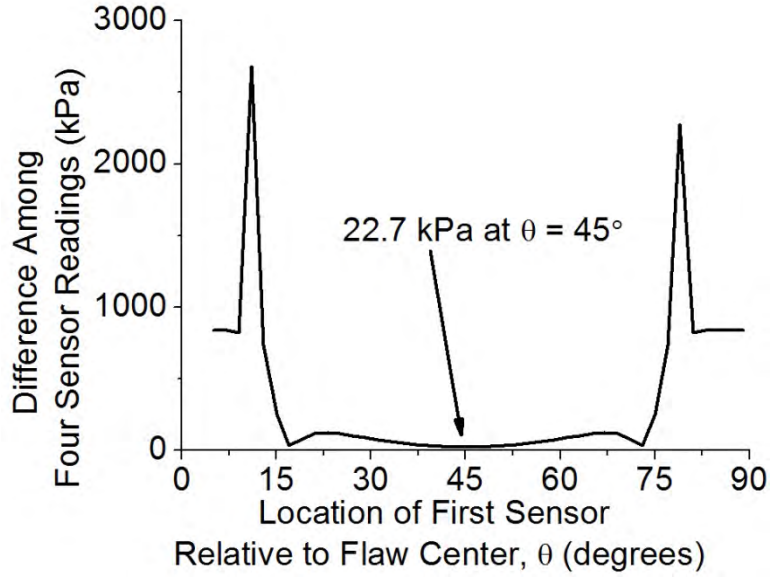

Figure 6: Differences among the four stress sensor readings as a function of position. The data shown is for a 20˚ debond angle at the -40˚C

Similar analyses were conducted for three-sensor and six-sensor systems. For the 20˚ debond angle, the difference between the maximum and minimum readings at the least-optimal locations were 21.0 kPa and 45.4 kPa respectively. By performing similar analyses (using the finite element models described above) for various debond angles, curves relating the detectable debond angle for three-, four-, and six-sensor systems were derived and used to construct a set of curves – these results are shown in Figure 7 below. The figure shows that increasing the number of sensors improves flaw detectability. For example, with six sensors, delaminations with total debond angles at or above 9˚ can be detected with 100% reliability. However, with three- or four sensor- systems, only debonds with angles of at least 15˚ can be detected with 100% reliability.

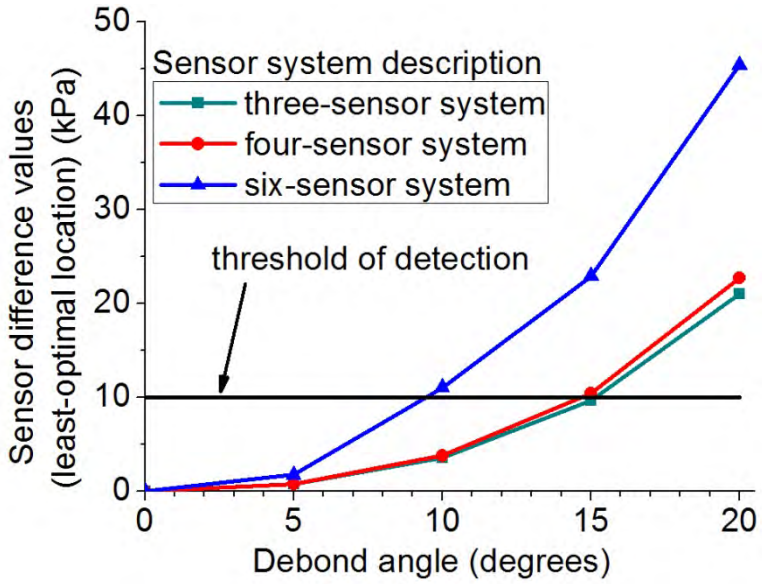

Figure 7: Relationship between stress differences (in the least optimal location) and detectable debond angle using various numbers of sensors

Figure 6 and 7 show results for debonds in a motor at -40˚C, however, the proposed health monitoring system can detect debonds at less extreme temperatures. To examine the effects of temperature on flaw detectability, a four-sensor system is assumed with an initial temperature of 60˚C and final temperatures of 20˚ C, 0˚ C, -20˚C and -40˚ C. The debond angle in this case is 20˚. This part of the analysis is summarized in Figure 8 below.

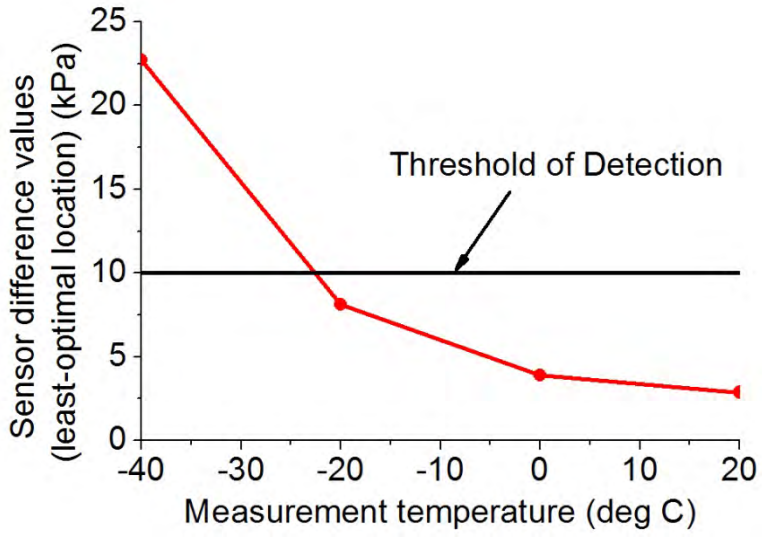

Figure 8: Stress differences in a four-sensor system at the least-optimal location at various temperatures

It is interesting to note that the debond detectability of the three- and four- sensor systems are very similar (see, for example, the two corresponding curves in Figure 7). On the surface, this suggests that a three-sensor system is ideal, since the results are very close. However, the situation if one sensor is allowed to fail is different. An analysis of the finite element data shows that if this occurs in a four-sensor

system, the stress difference (at the least optimal location) between the three remaining sensor readings is 14.4 kPa – so even with one of the four sensors not working, the 20˚ debond can still be detected with 100% probability of detection, assuming 10 kPa sensor accuracy. Figure 9 shows this analysis. Similarly, a three-sensor system was analyzed with a single sensor failure – in this case, the stress difference (at the least optimal location) was less 0.2 kPa (much less than the 10 kPa of sensor accuracy), so having two viable sensors in a three-sensor system is inadequate. The implication is that analyses need to be conducted that allow for failure of a sensor so that the health monitoring system is robust enough to perform well over the service life of the motor.

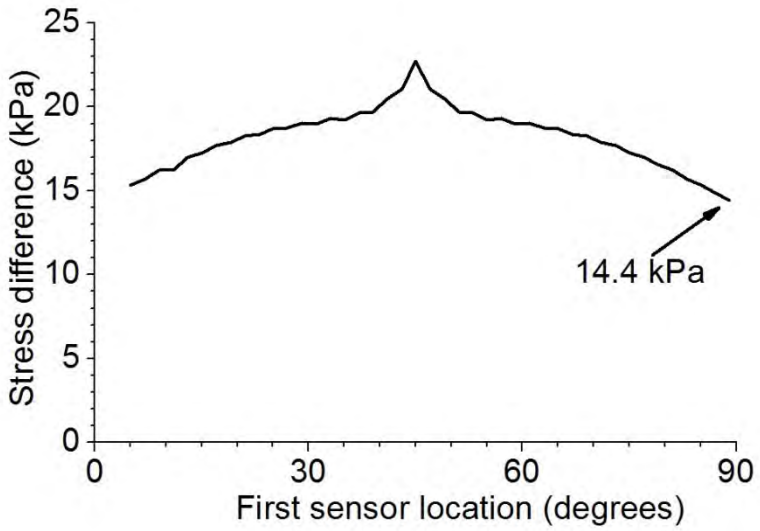

Figure 9: Stress differences for a four-sensor system assuming random failure of a single sensor

A Second Method to Detect Delaminations

In the previous text, we considered comparing different sensor readings on a motor to determine the possibility of delaminations – this could be called the “differential method.” Another approach, which we will call the “baseline method,” would be to compare the sensor readings with the readings from an unflawed motor. In this section, a four-sensor system with a temperature drop from 60˚C to -40˚C is considered using this “baseline method.” The following procedure is proposed. First, use finite elements to determine the radial stresses at the propellant/insulation interface in the flaw-free motor (this is called the “reference value”). Next, determine the largest variation from this reference value for various orientations of the system relative to the flaw. At the least-optimal location, the variation will indicate whether the debond can be detected with 100% reliability. This depends of course on the sensor accuracy and is a conservative prediction. The only caveat is that any shift in the reference value could affect the viability of the analysis, so if substantial shifts in the stress-free temperature are anticipated, the baseline method must be used with caution. Figure 10 shows that the “baseline method” works somewhat better than the “differential method” in such instances.

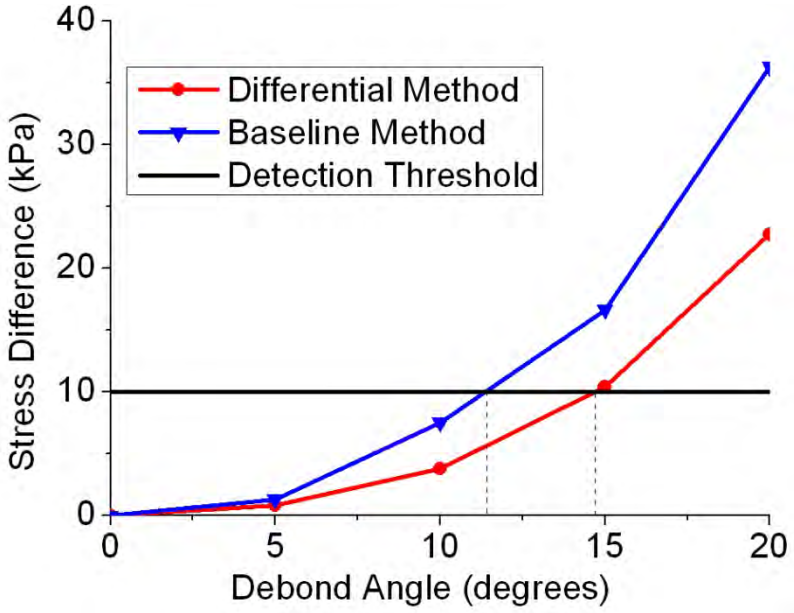

Figure 10: A comparison of flaw detectability using two different methods of detection

Previously, we analyzed data at the "least-optimal location," and this gave a conservative estimate of health monitoring system performance. However, this approach ignores most of the data – it is possible to use the entire data set (for example, the entire curve in Figure 6, as opposed to just its minimum) to determine a probability of detection for a flaw in a motor. For any given flaw size, some sensor orientations will have values greater than the sensor accuracy, and some will not. Probability of detection arises from a comparison of such a curve with the sensor accuracy level. Below, motors with a four-sensor system at -40˚C are analyzed. The following figure illustrates the probability of detection for each debond angle – again assuming a sensor accuracy of 10 kPa. Figure 11 shows that the probability of detection is similar for both methods.

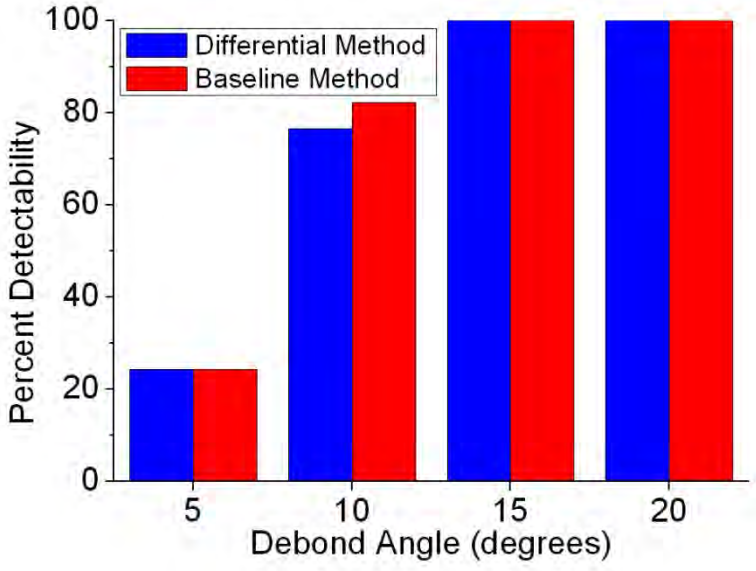

Figure 11: Detectability of flaws for the two proposed methods of analyzing data

Once the health monitoring data indicates a debond exists, the next question is: how large is the debond? The following method is proposed by the authors to estimate debond angles – in this case, we illustrate it with a four-sensor system and a temperature drop of 100˚C. This method focuses on the absolute difference between the two intermediate values of sensor readings (excluding the maximum and minimum values of sensor readings).

For each location of a set of four sensors, by using the finite element data, the sensors readings are arranged in decreasing order: R_1, R_2, R_3, and R_4. Figure 12 shows the range (scattered points) of the value ($R_2 – R_3$) as a function of debond angle. The solid lines in the figure represent the boundaries of maximum and minimum stress values of ($R_2 – R_3$) with all the debond angles considered (0˚ to 20˚). Therefore, at a given debond angle, the values of ($R_2 – R_3$) vary in a defined envelope. With no debond ($\alpha = 0$˚ in Figure 12), R_1, R_2, R_3, and R_4 are always equal, so the stress difference is zero – but this stress difference increases with the size of the debond. To use the graph, the value of ($R_2 – R_3$) is obtained from sensor readings and is referred to the y-component so that the corresponding upper and lower limits for the debond angle (x-components) can be estimated. For example, if the two stress readings R_2 and R_3 differ by 5 kPa, then the corresponding debond is between 11.5˚ and 16.5˚.

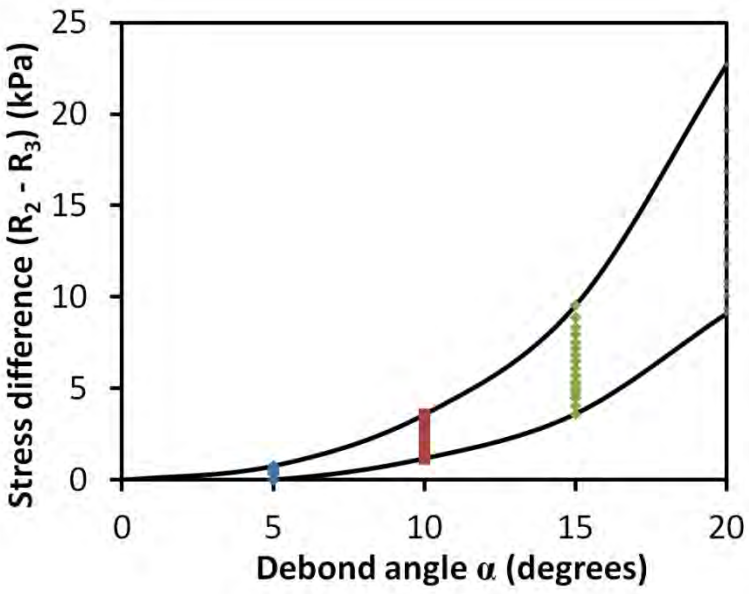

Figure 12: A method for determining the extent of the debond using four-sensor system data

CONCLUSIONS

Health monitoring sensor data can be used to detect delaminations (debonds) along the propellant/insulation interface in solid rocket motors. The sensors analyzed here measure bondline stresses and temperatures. We found that using the “baseline method” was preferable to the “differential method” if no stress-free temperatures shifts are anticipated – however, results were similar for both methods. Careful analysis of the data can show the minimum detectable debond in the motor. Conservative detectability predictions can be made by assuming the sensors are in the least-optimal location. Alternatively, a less conservative approach can be used which estimates probability of detection. Issues of redundancy were addressed and have been shown to be important (if a sensor fails, detectability can be affected). Finally, a quantitative relationship is established that allows estimation of the size of the debond from the sensor data. The approaches outlined in this paper should be applicable to specific motor configurations, and will help determine the optimum number of sensors and the detectability of flaws using such a sensor system.

ACKNOWLEDGEMENTS

This work was made possible by the U.S. Air Force Research Lab at Edwards Air Force Base (AFRL), which supported the Air Force Summer Faculty Fellowship Program (SFFP) administered by the American Society for Engineering Education (ASEE). The authors gratefully acknowledge technical assistance from Jim Buswell and Herb Chelner of Micron Instruments in regards to the dual bond stress and temperature (DBST) sensors and Greg Yandek of AFRL/RZSM for the data collection of EPDM insulation material.

REFERENCES

[1] Ruderman, G. A., "Health Management Issues and Strategy for Air Force Missiles," *International Forum on Integrated System Health Engineering and Management in Aerospace*, Napa, California, Nov. 7-10, 2005.

[2] Little, R.R., Chelner, H., Buswell, H.J., "Development, Testing, and Application of Embedded Sensors for Solid Rocket Motor Health Monitoring," *Proceedings of 37th Annual Conference of Fraunhofer-Institute for Chemical Technology (ICT)*, Karlsruhe, Germany, June 27-30, 2006, pp. 1-12.

[3] Ozupek, S., "Computational Procedure for the Life Assessment of Solid Rocket Motors," *AIAA Journal of Spacecraft and Rockets*, Vol. 47, 2010, pp. 639-648.

[4] Judge, M.D., "An Investigation of Composite Propellant Accelerated Ageing Mechanisms and Kinetics," *Propellants, Explosives, Pyrotechnics*, Vol. 28, 2003, pp. 114-118.

[5] Iqbal, M.M., Liang, W., "Modeling the Moisture Effects of Solid Ingredients on Composite Propellant Properties," *Aerospace Science and Technology*, Vol. 10, 2006, pp. 695-699.

[6] Brouwer, G., Weterings, F. P., and Keizers, H.L.J., "Evaluation of Ageing in Composite Propellant Grains," *41st AIAA Joint Propulsion Conference*, AIAA Paper 2005-3803, July 2005

[7] Brouwer, G.C.R., Buswell, H.J., Chelner, H., "The Use of Embedded Bond Stress Sensors to Determine Aging," *Proceedings of 43rd AIAA/ASME/SAE/ASEE Joint Propulsion Conference and Exhibit (AIAA-2007-5788)*, Cincinnati, OH, July 8-11, 2007, pp. 1-11.

[8] Cerri, S., Bohn, M.A., Menke, K., Galfetti, L., "Ageing Behaviour of HTPB Rocket Propellant Formulations," *Central European Journal of Energetic Materials*, Vol. 6, 2009, pp. 149-165.

[9] Ho, S.-Y., Care, G., "Modified Fracture Mechanics Approach in Structural Analysis of Solid-Rocket Motors," *AIAA Journal of Propulsion and Power*, Vol. 14, 1998, pp. 409-415.

[10] Wong, F.C., "Pseudodomain Fracture Analysis of Instrumented Analog Rocket Motors," *AIAA Journal of Spacecraft and Rockets*, Vol. 40, 2003, pp. 92-100.

[11] Tussiwand, G.S., Oley, D., Besser, H.-L., Weterings, F.P., Brouwer, G.C.R., "Application of Embedded Sensor Technology to a Full-Scale Experimental Nozzleless Rocket Motor," *Proceedings of 43rd AIAA/ASME/SAE/ASEE Joint Propulsion Conference and Exhibit (AIAA-2007-5790)*, Cincinnati, OH, July 8-11, 2007, pp. 1-18.

[12] Brouwer, G.C.R., Pfiffer, A., Bancallari, L., "Development and Deployment of Diagnostic Prognostic Tactical Solid Rocket Motor Demonstrator," *Proceedings of 47th AIAA/ASME/SAE/ASEE Joint Propulsion Conference and Exhibit (AIAA-2011-5788)*, San Diego, CA, July 31-August 3, 2011, pp. 1-11

[13] Delmonte, J., *Technology of Carbon and Graphite Fiber Composites*, Van Nostrand Reihold Company, New York, 1981, pp. 198-250.

[14] *ABAQUS Analysis User's Manual, Version 6.6*, ABAQUS, Inc., Providence, RI, 2006.

[15] Chelner, H., "Embedded Sensor Technology for Solid Rocket Motor Health Monitoring," SBIR Phase I Final Report, Contract No. DAAH01-02-R099, U. S. Army Aviation and Missile Command, Redstone Arsenal, Huntsville, Alabama, February 2003.

[16] Buswell, H. J., "Lessons Learned from Health Monitoring of Rocket Motors," *Proceedings of 41st AIAA/ASME/SAE/ASEE Joint Propulsion Conference and Exhibit (AIAA-2005-4558)*, Tucson, ,AZ, July 10-13, 2005.

AFRL

THE AIR FORCE RESEARCH LABORATORY

LEAD | DISCOVER | DEVELOP | DELIVER

DETECTABILITY OF DELAMINATIONS IN ROCKET MOTORS WITH EMBEDDED STRESS SENSORS

JANNAF S&MBS Meeting
30 April – 4 May 2012

Anhduong Q. Le and L. Z. Sun

University of California, Irvine, CA 92697-2175

Timothy C. Miller

Air Force Research Laboratory, Edwards AFB, CA 93524

Introduction

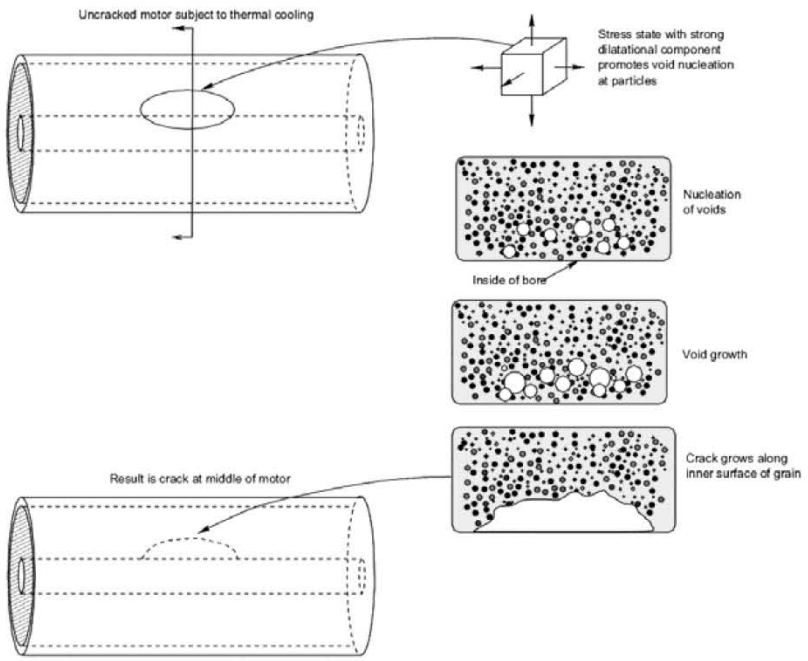

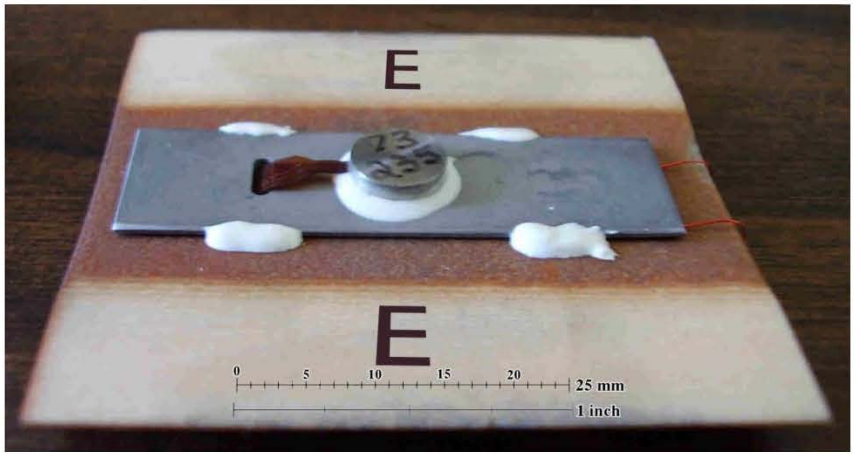

Introduction (Continued)

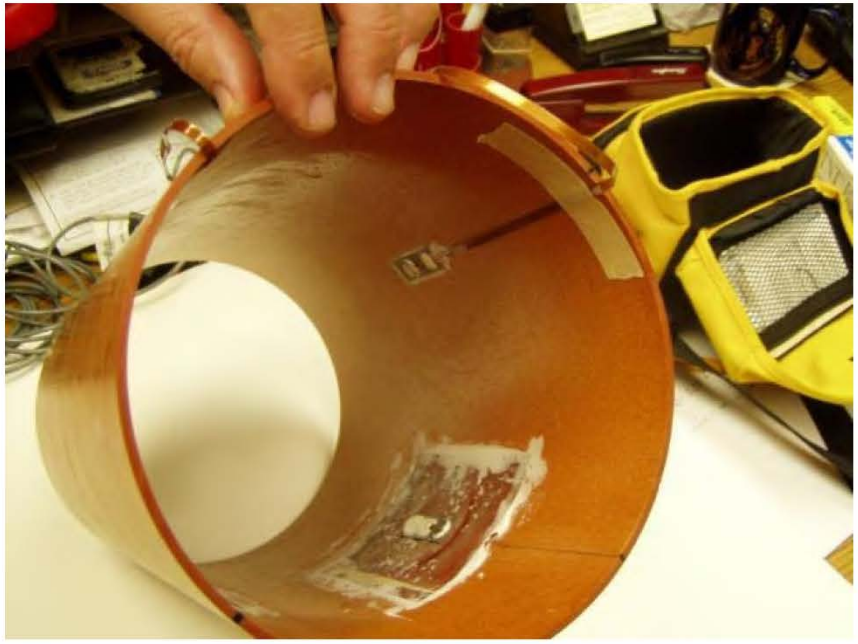

Finite Element Model Details

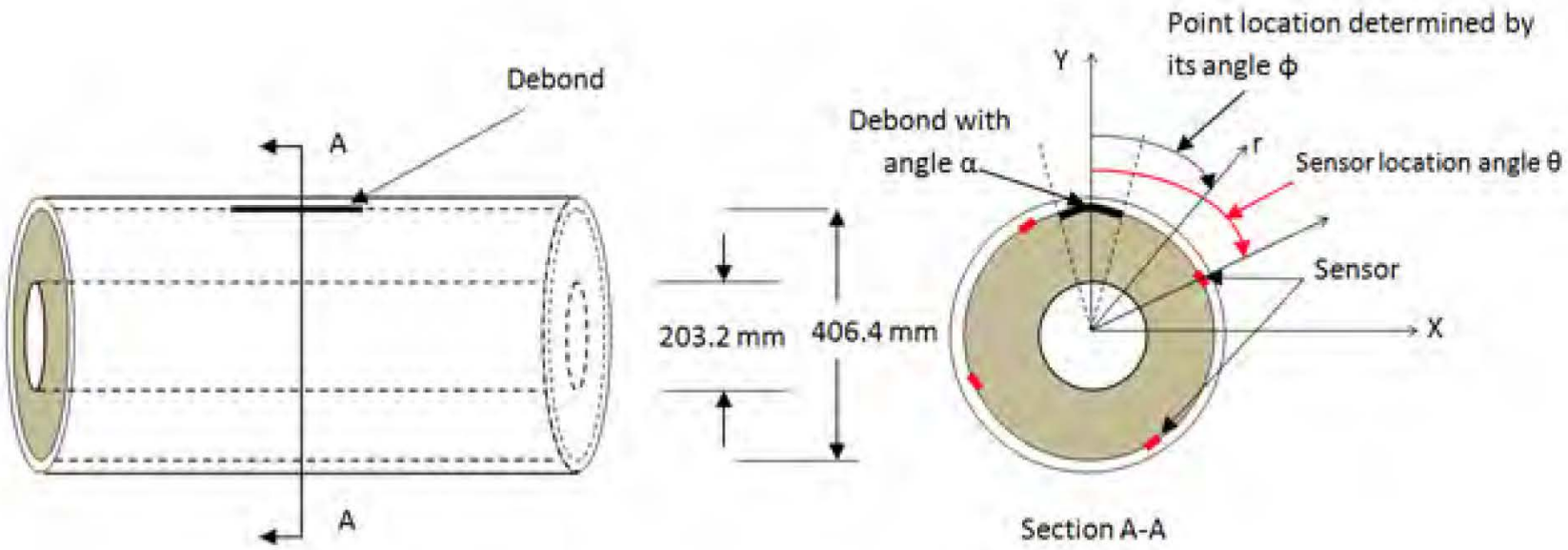

Finite Element Model Details (Continued)

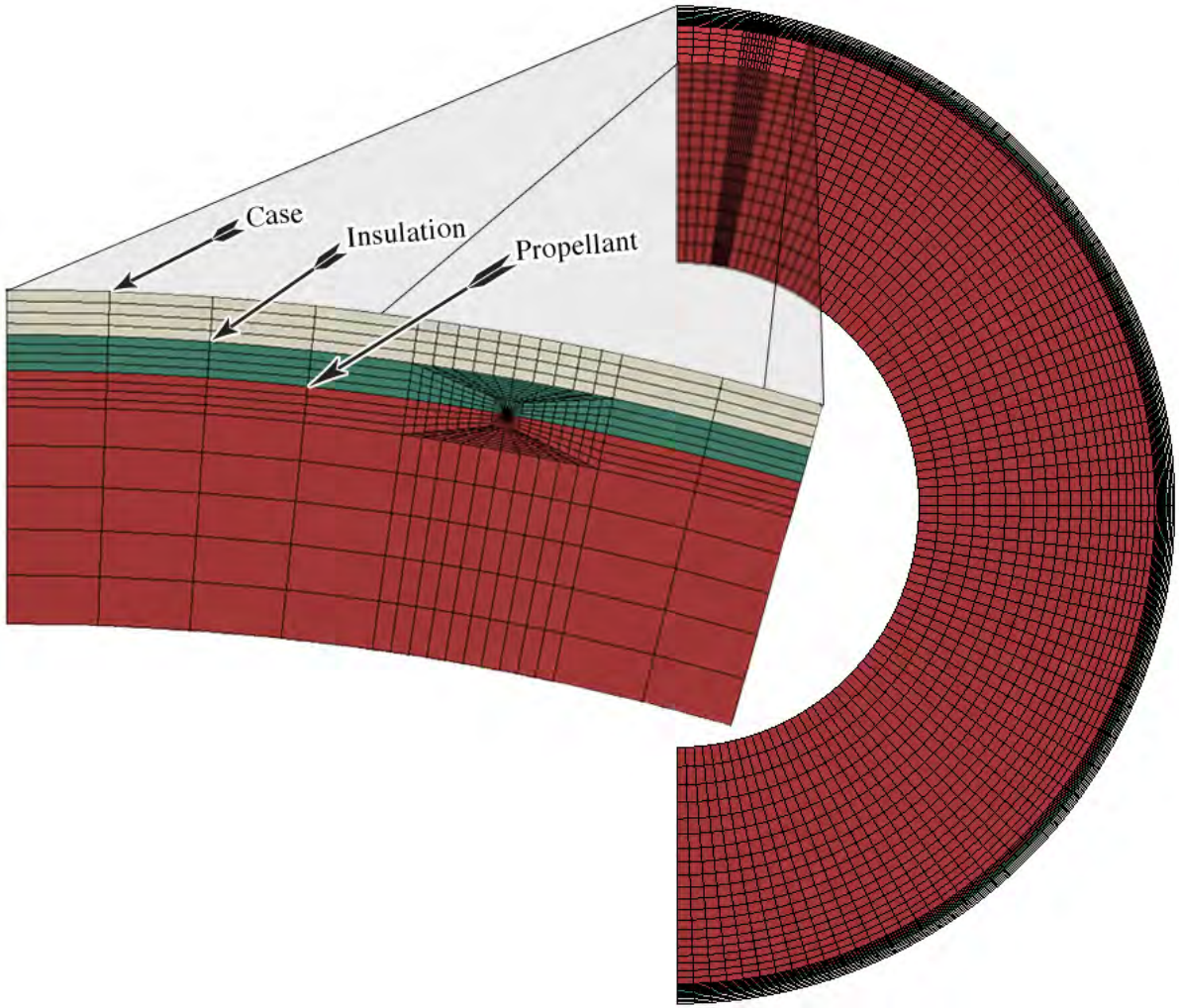

Case: Graphite-epoxy motor case, quasi-isotropic, linear elastic

Insulation: EPDM, temperature-dependent linear elastic

Grain: HTPB, temperature-dependent linear elastic

Results and Discussion
Contour Plots

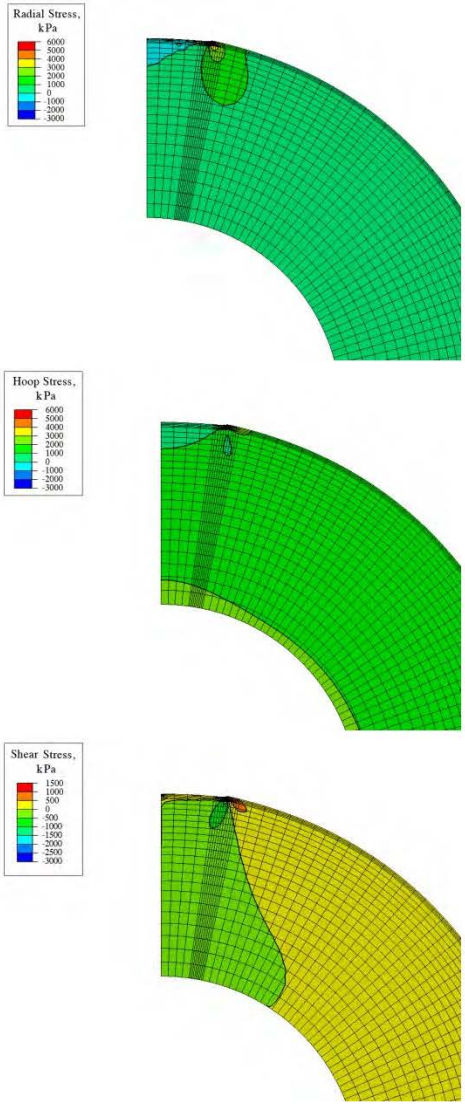

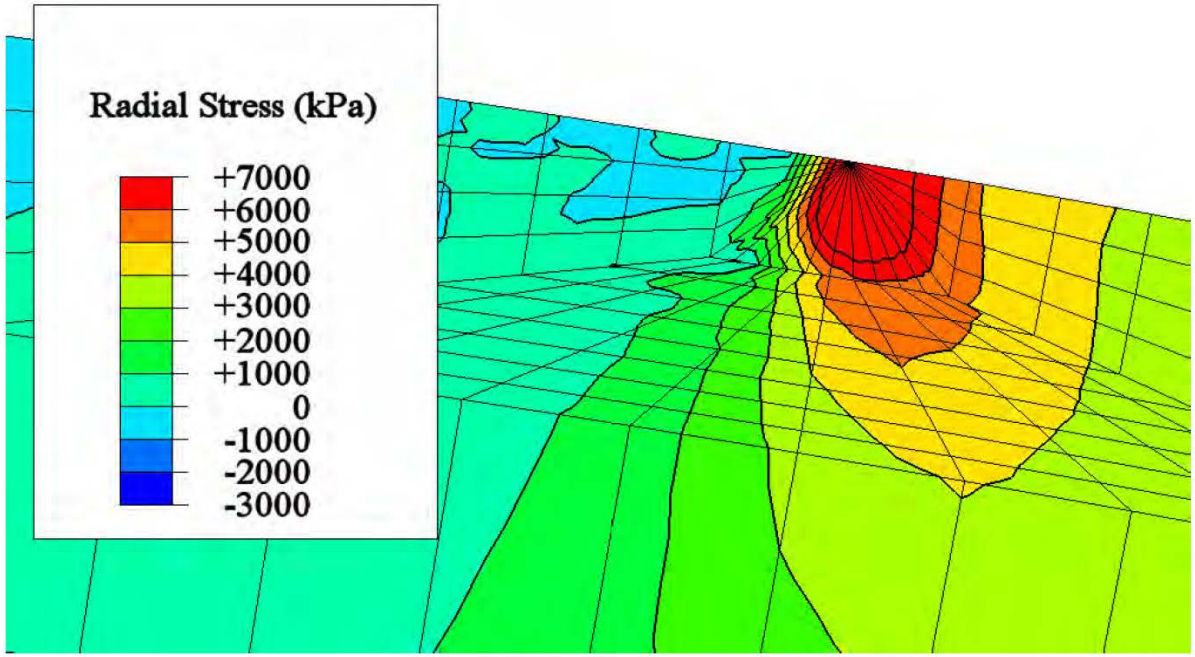

Results and Discussion
Case-Wall Radial Stresses

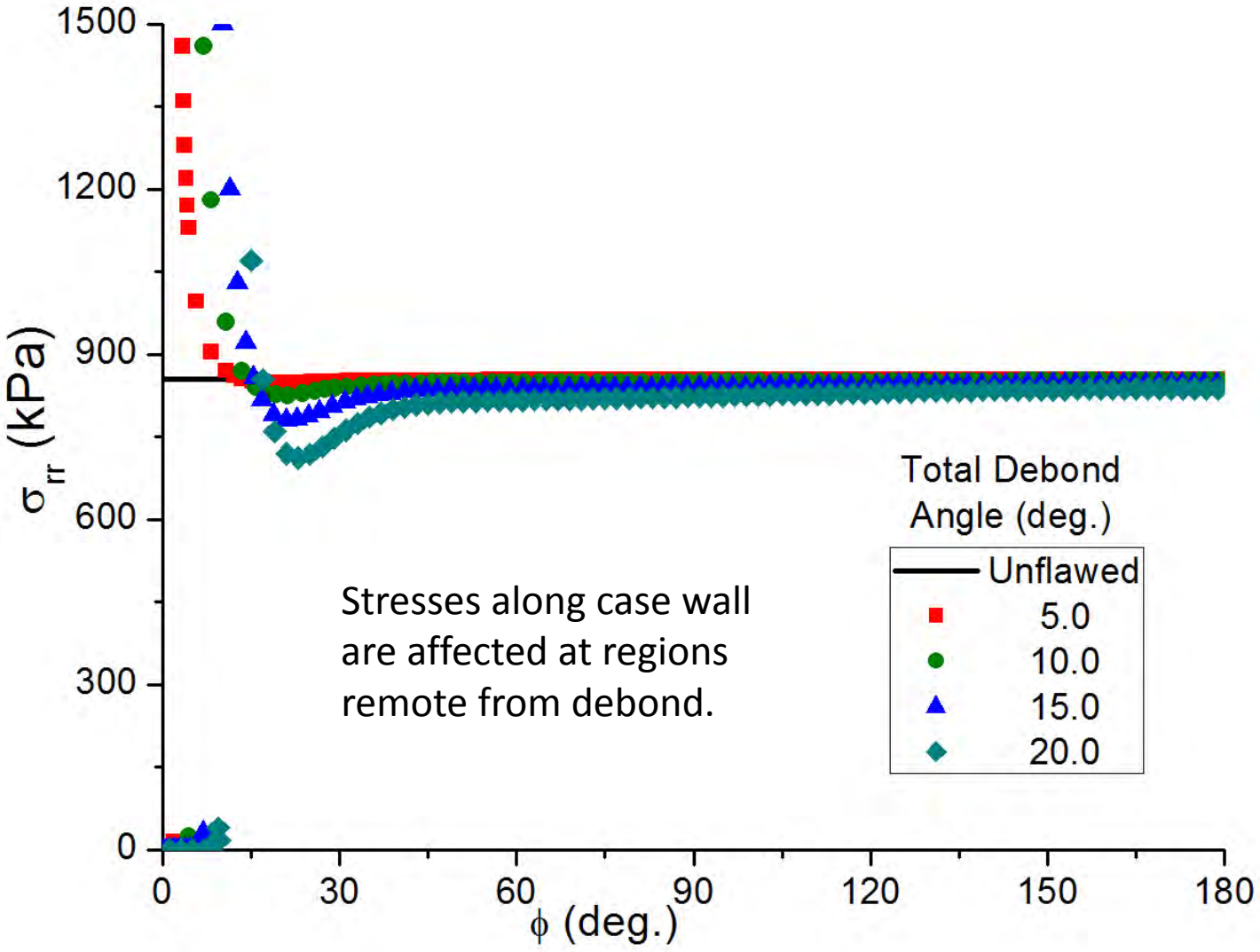

Results and Discussion
Differential Method

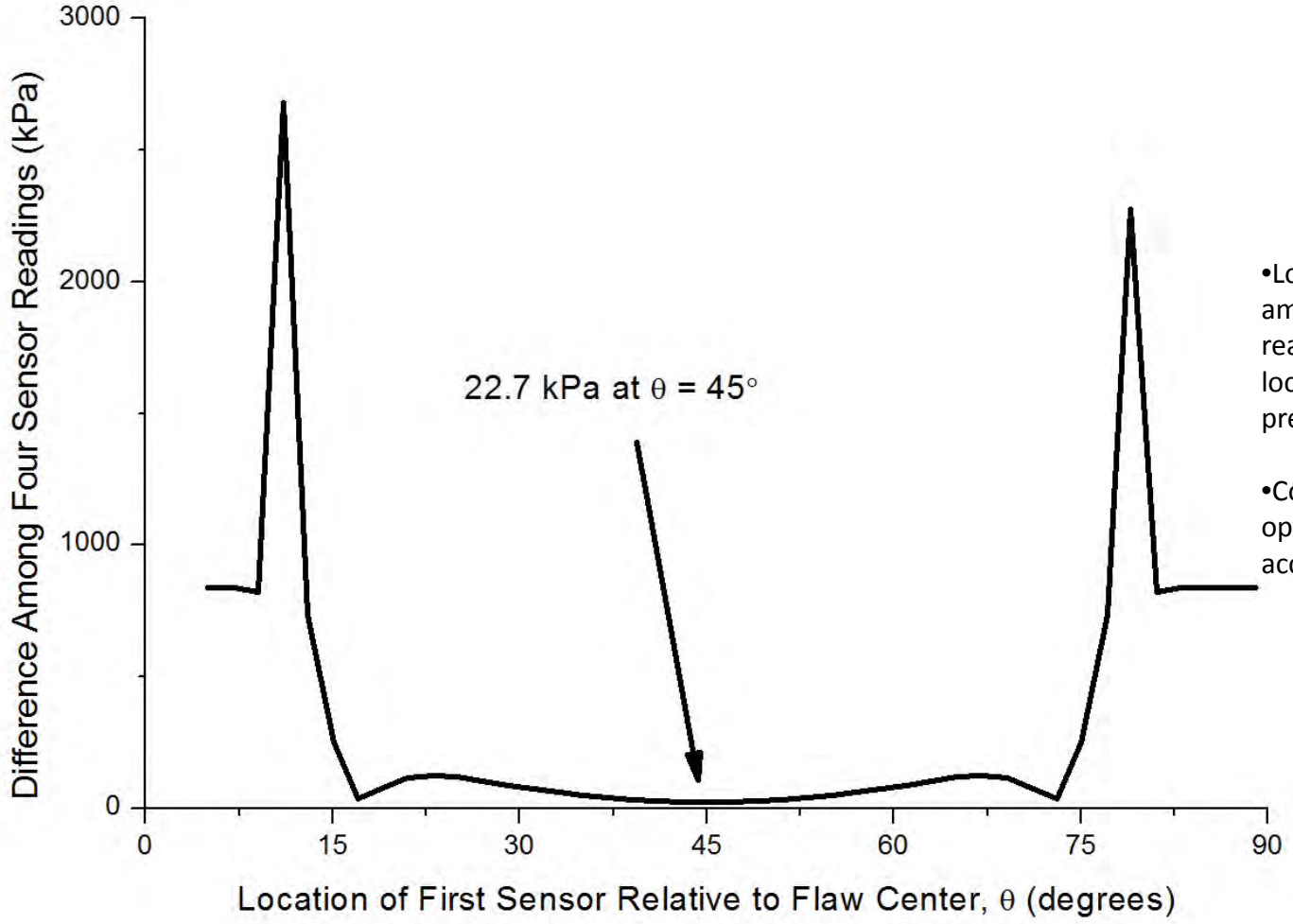

- Looking at the difference among the (four) sensor readings at "least-optimal" location gives conservative prediction of detectability.
- Compare reading at "least-optimal" location with sensor accuracy (10 kPa or less)

Results and Discussion
Differential Method

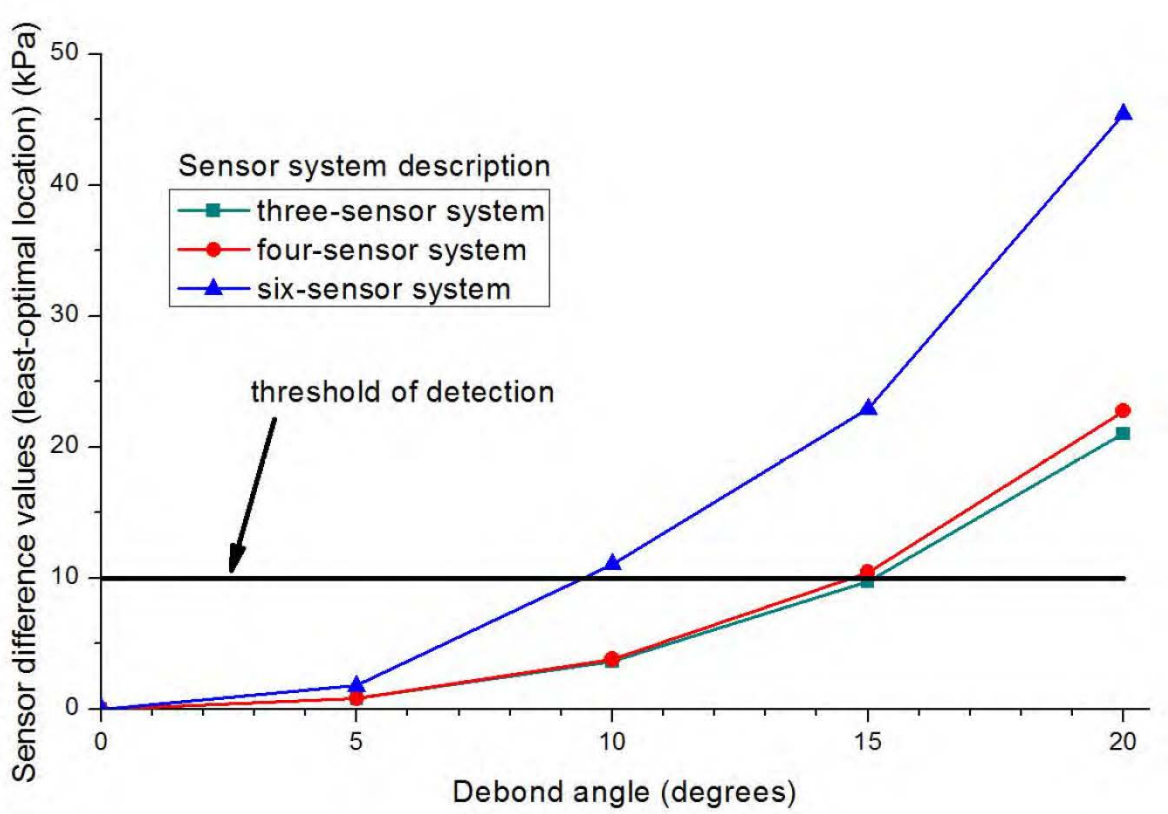

Results and Discussion
Baseline Method

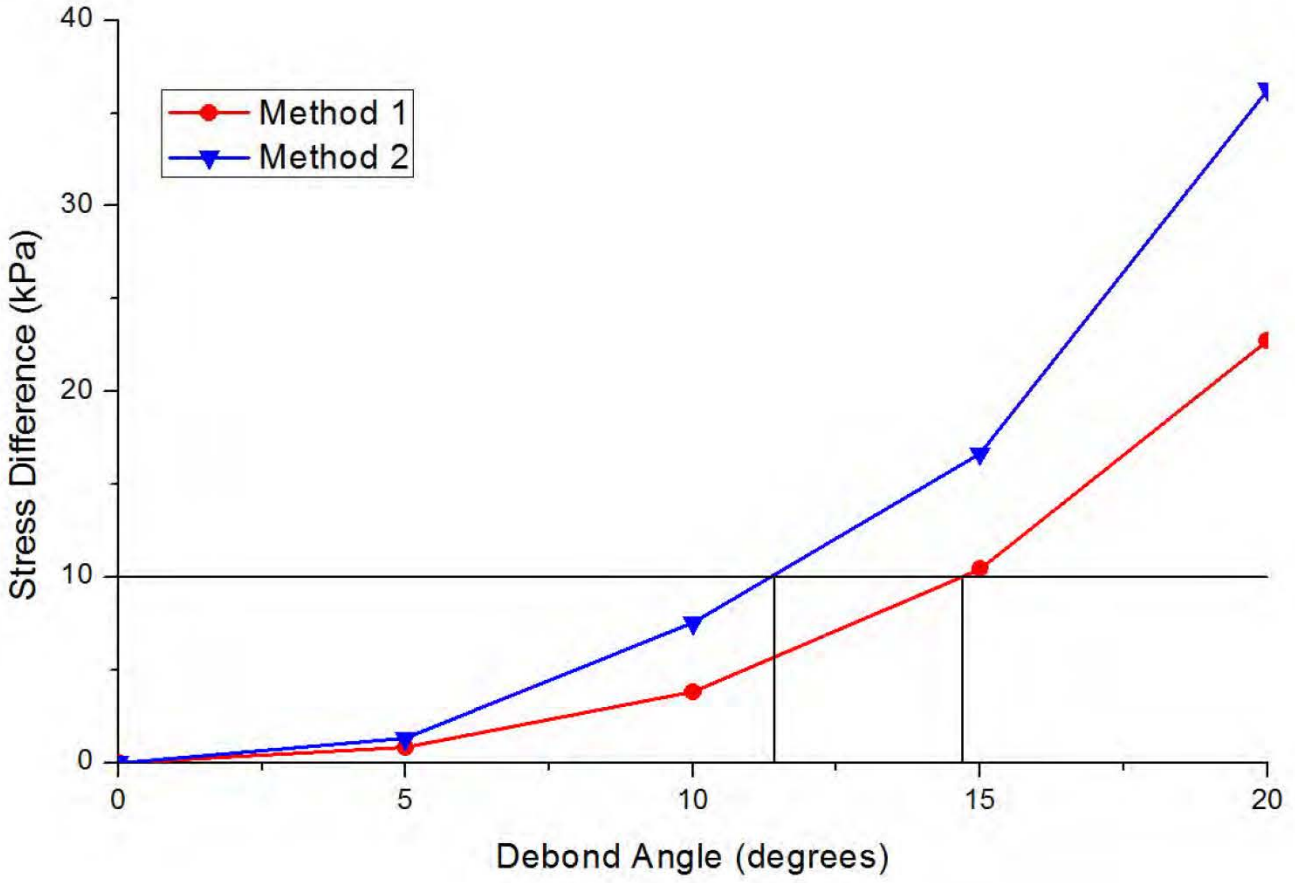

Results and Discussion
Effect of Test Temperature

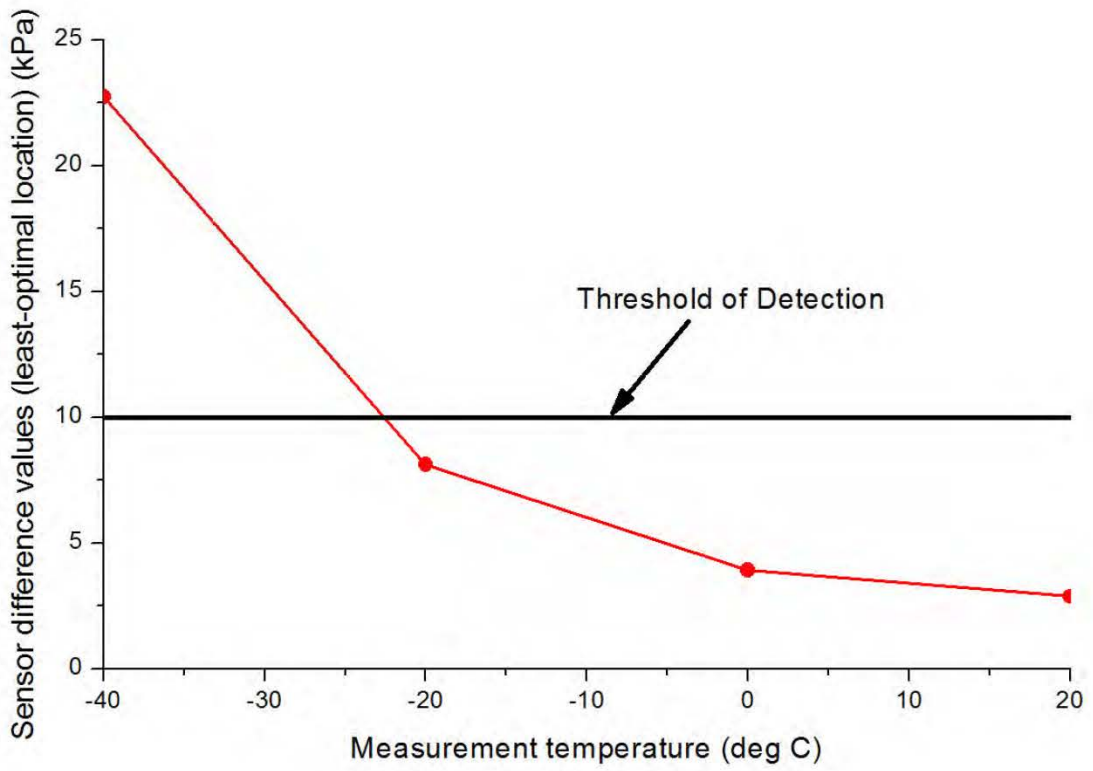

Results and Discussion
Effects of Sensor Failure

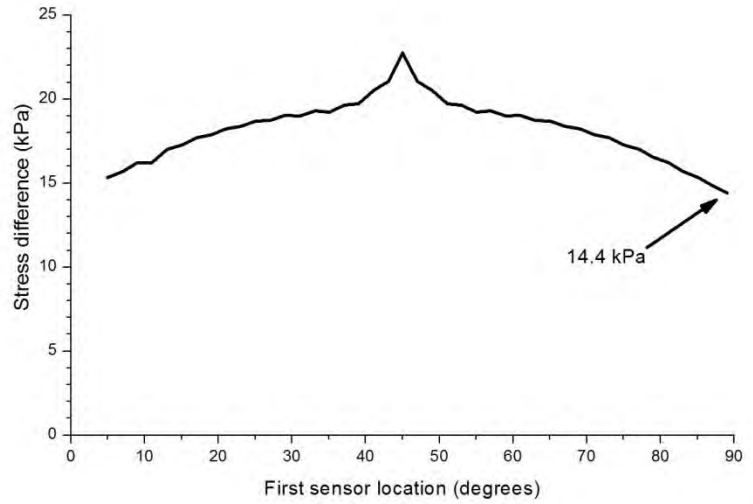

Four-sensor system with one failure:
Stress difference at “least-optimal” location = 14.4 kPa

Three-sensor system with one failure:
Stress difference at “least-optimal” location = 0.2 kPa

Results and Discussion
Probability of Detection

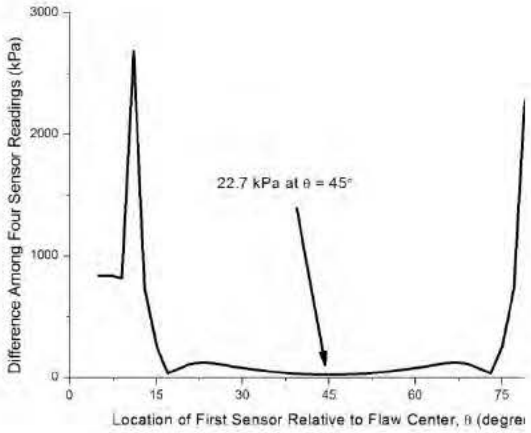

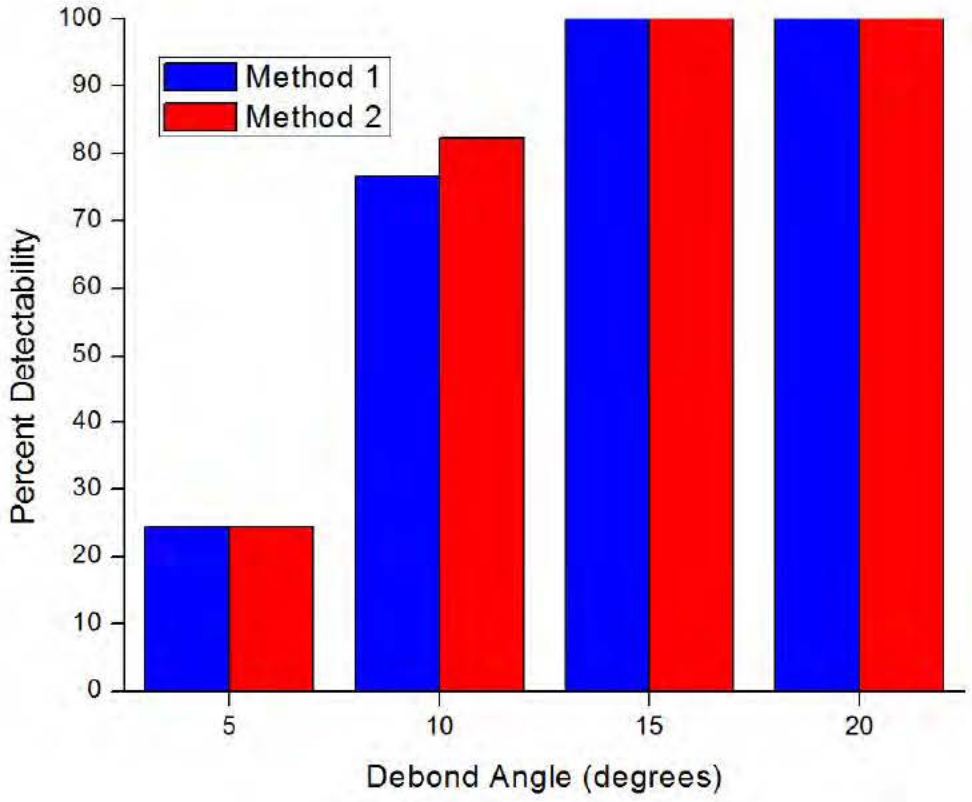

Results and Discussion
Estimation of Total Debond Angle

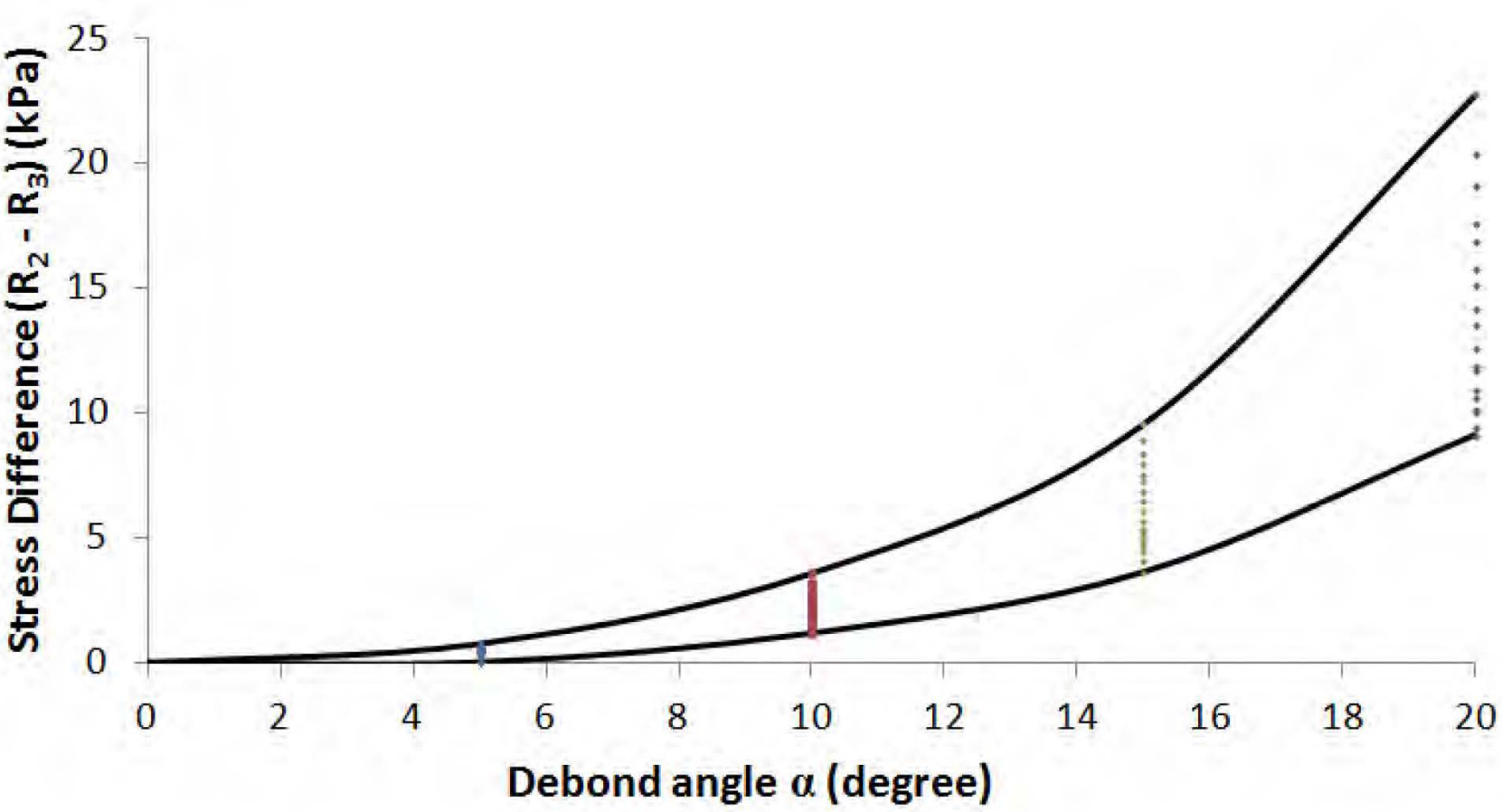

Conclusions

- **FEA analysis shows that debonds can be detected with pressure sensors at the case wall. Methodology is described, including:**
  - Differential and baseline methods
  - Effects of test temperature
  - Effects of sensor failure
  - Probability of detection
  - Method to estimate debond size